

Model-Free Prediction of Adversarial Drop Points in 3D Point Clouds

Hanieh Naderi, *Student Member, IEEE*, Chinthaka Dinesh, *Member, IEEE*, Ivan V. Bajić, *Senior Member, IEEE*, and Shohreh Kasaei, *Senior Member, IEEE*

Abstract—Adversarial attacks pose serious challenges for deep neural network (DNN)-based analysis of various input signals. In the case of 3D point clouds, methods have been developed to identify points that play a key role in the network decision, and these become crucial in generating existing adversarial attacks. For example, a saliency map approach is a popular method for identifying adversarial drop points, whose removal would significantly impact the network decision. Generally, methods for identifying adversarial points rely on the deep model itself in order to determine which points are critically important for the model’s decision. This paper aims to provide a novel viewpoint on this problem, in which adversarial points can be predicted independently of the model. To this end, we define 14 point cloud features and use multiple linear regression to examine whether these features can be used for model-free adversarial point prediction, and which combination of features is best suited for this purpose. Experiments show that a suitable combination of features is able to predict adversarial points of three different networks – PointNet, PointNet++, and DGCNN – significantly better than a random guess. The results also provide further insight into DNNs for point cloud analysis, by showing which features play key roles in their decision-making process.

Index Terms—Point cloud processing, adversarial example, attack, graph signal processing, multiple linear regression.

I. INTRODUCTION

Deep Neural Networks (DNNs) have made outstanding contributions to various computer vision tasks due to their ability to model complex input-output relationships from a relatively limited set of data. However, studies have shown that DNNs are severely vulnerable to adversarial examples [1], [2]. An adversarial example is an input to a model that is carefully designed to cause the model to make a wrong decision. A great deal of literature has been devoted to constructing 2D adversarial examples and exploring related defenses [1]–[4]. The research scope of adversarial attacks has gradually expanded to include 3D point clouds in addition to 2D images [5], [6].

Given a deep model for point cloud analysis, a number of methods have been proposed to determine critical points that could be used in an adversarial attack [7]–[9]. For example, Zheng *et al.* [7] proposed a differentiable method of point shifting towards the cloud center, known as a *saliency map*

technique, which approximates point dropping and assigns contribution scores to input points based on the resulting loss value. Other methods for determining critical points similarly try to estimate the effect of point disturbance on the output.

Once the critical points have been determined, they can be used to create adversarial examples. Several recent studies [5], [6], [10] use the critical points as initial positions and then introduce perturbations to create attacks. Usually, some distance-related criteria, such as Hausdorff [6] or Chamfer distance [6], are used to constrain the perturbations around critical positions. Instead of perturbation, another kind of attack drops the critical points; for example, the well-known Drop100 and Drop200 attacks [7] drop, respectively, 100 and 200 points from the point cloud in order to force the model to make a wrong decision. These are considered among the most challenging attacks to defend against [5], [11]–[13].

The above-mentioned methods, and others in the literature, require the knowledge of the DNN model in order to determine critical points. Such approaches are in line with the popular view in the literature [2]: that the existence of adversarial examples is a *flaw of the model*, that they exist because the model is overly parametrized, nonlinear, etc. According to this reasoning, each model has its own flaws, i.e., its own critical points. Another view is that adversarial examples are consequences of the data distribution on which the model is trained [14]. This would suggest that different models trained on the same data may share some adversarial examples, but they have to be determined in the context of the data distribution.

In this paper we present a different point of view. We show that it is possible to determine critical points in point clouds from the features of the point cloud itself, without using the target DNN model (a “model-free” approach) or the data distribution. This would suggest that critical points in point clouds are not only consequences of the flaws of deep models, nor the data distribution, but also inherent characteristics of the point clouds themselves, which give them their crucial properties that are important in their analysis, i.e., what makes an airplane - an airplane, or a chair - a chair.

The rest of the paper is organized as follows. The related work is discussed in Section II, along with further explanation of our contribution. Our proposed fourteen point cloud features are presented in Section IV and their multiple linear regression analysis in Section IV. Experimental results are reported in Section V, followed by conclusions in Section VI.

Hanieh Naderi and Shohreh Kasaei are with the Department of Computer Engineering, Sharif University of Technology Tehran, Iran, e-mail: kasaei@sharif.edu.

Chinthaka Dinesh and Ivan V. Bajić are with the School of Engineering Science, Simon Fraser University, Burnaby, BC, Canada, e-mail: ibaji@ensc.sfu.ca.

This work has been supported in part by the Iran National Science Foundation (INSF) and the Natural Sciences and Engineering Research Council (NSERC) of Canada.

II. RELATED WORK

A. Deep models for point cloud analysis

PointNet [15] was a pioneering approach for DNN-based point cloud analysis. Learnt features are extracted from individual points in the input point cloud and then aggregated to global features via max-pooling. As a result of these global features, a shape can be summarized by a sparse set of key points, also called the *critical point set*. The authors of PointNet showed that any set of points between the critical point set and another set called the *upper bound shape* will give the same set of global features, and thus lead to the same network decision. While this proved a certain level of robustness of PointNet to input perturbations, it also pointed to strong reliance on the critical point set, which was subsequently used to design various adversarial attacks.

PointNet has inspired much subsequent work on DNN-based point cloud analysis, of which we review only two approaches subsequently used in our experiments. One of these is PointNet++ [16], a hierarchical network designed to capture fine geometric structures in a point cloud. Three layers make up PointNet++: the sampling layer, the grouping layer, and the PointNet-based learning layer. These three layers are repeated in PointNet++ to learn local geometric structures. Another representative work is Dynamic Graph Convolutional Neural Network (DGCNN) [17]. It exploits local geometric structures by creating a local neighborhood graph and using convolution-like operations on the edges connecting neighboring pairs of points.

B. Adversarial attacks on point clouds

Point clouds are defined by the 3D coordinates of points making up the cloud. Thus, adversarial attacks can be performed by adding, dropping, or shifting points in the input cloud. An adversarial attack can be created by examining all points in the input cloud, or just critical points as potential targets. Liu *et al.* [5] were inspired by the success of gradient-guided attack methods, such as Fast Gradient Sign Method (FGSM) [1] and Projected Gradient Descent (PGD) [18], on 2D images. They applied similar methodology to develop adversarial attacks on 3D point clouds. Similarly, the Carlini and Wagner (C&W) [4] optimization for finding adversarial examples has also been transplanted to 3D data. For example, Tsai *et al.* [19] use the C&W optimization formulation with an additional perturbation-bound regularization to construct adversarial attacks. To generate an attack with a minimum number of points, Kim *et al.* [20] extend the C&W formulation by adding a term to constrain the number of perturbed points. The adversarial points found in [20] were almost identical to the PointNet critical points.

Xiang *et al.* [6] demonstrated that PointNet can be fooled by shifting or adding synthetic points, or adding clusters and objects to the point cloud. To find such adversarial examples, they applied the C&W strategy to the critical points, rather than all points. Constraining the search space around critical points is sometimes necessary, because an extensive search through an unconstrained 3D space is infeasible. An attack

method that uses the critical-point property for PointNet is proposed by Yang *et al.* [10]. By recalculating the class-dependent importance for each remaining point, they iteratively remove the most crucial point for the true class. The authors stated that the critical points exist in different models and that a universal point-dropping method should be developed for all models. Wicker *et al.* [21] proposed randomly and iteratively determining the critical points and then generating adversarial examples for attack by dropping these points.

Arya *et al.* [22] identify critical points by calculating the largest magnitudes of the loss gradient with respect to the points. After finding those points, the authors propose a minimal set of adversarial points among critical points and perturb them slightly to create adversarial examples. Zheng *et al.* [7] developed a more flexible method that extends finding critical points to other deep models besides PointNet. They introduced a *saliency score* defined as

$$s_i = -r_i^{1+\alpha} \frac{\partial \mathcal{L}}{\partial r_i}, \quad (1)$$

where r_i is the distance of the i -th point to the cloud center, α is a hyperparameter, and $\frac{\partial \mathcal{L}}{\partial r_i}$ is the gradient of the loss \mathcal{L} with respect to the amount of shifting the point towards the center. Adversarial examples are created by shifting the points with high saliency scores towards the center, so that they will not affect the surfaces much.

Besides the methods for creating adversarial attacks on point clouds, a number of methods for defending against these attacks have been developed. For 3D point cloud classification, removing points as a pre-processing step in training was shown to be more effective than adversarial training [23]. Some of the methods proposed for point removal to improve robustness against adversarial attacks include simple random sampling (SRS) [10], statistical outlier removal (SOR) [13], Denoiser and Upsampler Network (DUP-Net) [13], high-frequency removal [12], and salient point removal [5].

C. Our contribution

We focus on adversarial drop attacks, and subsequently refer to the corresponding critical points as *adversarial drop points*. We define a set of fourteen point cloud features and examine which features can be used to predict adversarial drop points derived from three different deep models – PointNet [15], PointNet++ [16], and DGCNN [24]. Using multiple linear regression, we identify a set of features that appear to be highly explanatory in terms of their ability to predict adversarial drop points. We also show that using a combination of these features, we are able to predict adversarial drop points in a specific point cloud much better than a random guess, for each of the three deep models mentioned above.

III. POINT CLOUD FEATURES

In this section, leveraging on recent advances in *graph signal processing* (GSP) [25], [26]—a fast-growing field in the signal processing community studying signals residing on irregular domains modeled as graphs—we computed a set of graph-based features to predict adversarial drop points in 3D

point clouds based on multiple linear regression. Therefore, first, we review the basic concepts in GSP and the graph construction for a given 3D point cloud, which will lead to computing the graph-based features.

A. Preliminaries

1) *Graph definitions:* A undirected weighted graph $\mathcal{G} = (\mathcal{V}, \mathcal{E}, \mathbf{W})$ is defined by a set of N nodes $\mathcal{V} = \{1, \dots, N\}$, edges $\mathcal{E} = \{(i, j)\}$, and a symmetric adjacency matrix \mathbf{W} . $W_{i,j} \in \mathbb{R}^+$ is the edge weight if $(i, j) \in \mathcal{E}$, and $W_{i,j} = 0$ otherwise. Diagonal degree matrix \mathbf{D} has diagonal entries $D_{i,i} = \sum_j W_{i,j}, \forall i$. A combinatorial graph Laplacian matrix \mathbf{L} is defined as $\mathbf{L} \triangleq \mathbf{D} - \mathbf{W}$ [27]. Further, a transition matrix \mathbf{A} is defined as $\mathbf{A} \triangleq \mathbf{D}^{-1}\mathbf{W}$ [28]. By definition $\sum_{j \in \mathcal{N}_i} A_{i,j} = 1$. In general, a vector $\mathbf{x} = [x_1 \dots x_N]^\top \in \mathbb{R}^V$ can be interpreted as a graph signal, where x_i is a scalar value assigned to node $i \in \mathcal{V}$. Further, for given graph signal \mathbf{x} , a weighted average signal value at node i around its neighbours can be computed as

$$\bar{x}_i = (\mathbf{A}\mathbf{x})_i = \sum_{j \in \mathcal{N}_i} A_{i,j} x_j, \quad (2)$$

where \mathcal{N}_i is the 1-hop neighborhoods of node i . Moreover, the second difference of the graph signal \mathbf{x} at node i is given as

$$\tilde{x}_i = (\mathbf{L}\mathbf{x})_i = L_{i,i} x_i + \sum_{j \in \mathcal{N}_i} L_{i,j} x_j. \quad (3)$$

2) *Graph construction for a 3D point cloud:* To enable graph-based feature-extraction of n 3D points, we first construct a neighborhood graph. In particular, we construct an undirected positive graph $\mathcal{G} = (\mathcal{V}, \mathcal{E}, \mathbf{W})$ composed of a node set \mathcal{V} of size n (each node represents a 3D point) and an edge set \mathcal{E} specified by $(i, j, W_{i,j})$, where $i \neq j, i, j \in \mathcal{V}$ and $W_{i,j} \in \mathbb{R}^+$. We connect each 3D point (graph node) to its k nearest neighbors j in Euclidean distance, so that each point can be filtered with its k neighboring points under a graph-structured data kernel [27], [29].

In the graph-based point cloud processing literature [30]–[33], using pairwise Euclidean distance $\|\mathbf{p}_i - \mathbf{p}_j\|_2^2$ to compute edge weight $W_{i,j}$ between nodes i and j is popular, i.e.,

$$W_{i,j} = \exp \left\{ -\frac{\|\mathbf{p}_i - \mathbf{p}_j\|_2^2}{\sigma_p^2} \right\}, \quad (4)$$

where $\mathbf{p}_i \in \mathbb{R}^3$ is the 3D coordinate of point i and σ is a parameter. In numerous graph-based point cloud processing works [30]–[32], [34]–[36], σ was manually chosen so that edge weight $W_{i,j}$ is large (close to 1) if 3D points i, j are physically close, and small (close to 0) otherwise.

B. Graph-based feature extraction

Based on these notions, we compute three sets of features for each 3D point in a given point cloud as follows.

1) *3D point coordinates-based features:* Denote by $\mathbf{P} = [\mathbf{p}_x; \mathbf{p}_y; \mathbf{p}_z] \in \mathbb{R}^{n \times 3}$, where \mathbf{p}_x , \mathbf{p}_y , and \mathbf{p}_z are x -, y -, and z -coordinates of the 3D points of the given point cloud. Here, we consider \mathbf{p}_x , \mathbf{p}_y , and \mathbf{p}_z as three graph signals on graph \mathcal{G} constructed from a given point cloud as in Section III-A2. Therefore, using (2), one can easily compute the weighted average 3D coordinate at node i as follows:

$$\bar{\mathbf{p}}_i = \left((\mathbf{A}\mathbf{P})^\top \right) (:, i) = \sum_{j \in \mathcal{N}_i} A_{i,j} \mathbf{p}_j, \quad (5)$$

where $\left((\mathbf{A}\mathbf{P})^\top \right) (:, i)$ is the i th column of $(\mathbf{A}\mathbf{P})^\top$. Further, according to (3), we can write the second difference of 3D coordinates \mathbf{P} at node i as follows:

$$\tilde{\mathbf{p}}_i = \left((\mathbf{L}\mathbf{P})^\top \right) (:, i) = L_{i,i} \mathbf{p}_i + \sum_{j \in \mathcal{N}_i} L_{i,j} \mathbf{p}_j. \quad (6)$$

Now, we consider x -, y -, and z -coordinates $\bar{\mathbf{p}}_i$ and $\tilde{\mathbf{p}}_i$ are one set of graph-based features at point i .

2) *Local variation-based features:* Similar to [28], local variation at point i can be quantified as:

$$v_i = \|\mathbf{p}_i - \bar{\mathbf{p}}_i\|_2, \quad (7)$$

where $\bar{\mathbf{p}}_i$ is in (5). Here, one can easily see that v_i is the Euclidean distance between point \mathbf{p}_i and the weighted average of its neighbors. Therefore, when the value of v_i is high, the point p_i cannot be well approximated from those of its neighboring points, and hence the point \mathbf{p}_i is thus likely to be a point of a edge, corner, or valley.

Further, we consider $\mathbf{v} = [v_1 \dots v_n]^\top$ as a graph signal of the graph \mathcal{G} constructed from the given point cloud as discussed in Section III-A2. Then, according to (2), weighted average signal value at node i is given as:

$$\bar{v}_i = \sum_{j \in \mathcal{N}_i} A_{i,j} v_j. \quad (8)$$

Using (3), second difference of signal \mathbf{v} at node i is given as:

$$\tilde{v}_i = L_{i,i} v_i + \sum_{j \in \mathcal{N}_i} L_{i,j} v_j. \quad (9)$$

Now, we consider v_i , \bar{v}_i and \tilde{v}_i are the second set of graph-based features at point i .

3) *Low-pass filter-based features:* For graph signals \mathbf{p}_x , \mathbf{p}_y , \mathbf{p}_z with respect to the graph \mathcal{G} , the corresponding low-pass filter (LPF) signals \mathbf{q}_x^* , \mathbf{q}_y^* , \mathbf{q}_z^* can be obtained by minimizing the following optimization problem (See [37] for details):

$$\mathbf{q}^* = \arg \min_{\mathbf{q}} \|\mathbf{p} - \mathbf{q}\|_2^2 + \gamma (\mathbf{q}_x^\top \mathbf{L} \mathbf{q}_x + \mathbf{q}_y^\top \mathbf{L} \mathbf{q}_y + \mathbf{q}_z^\top \mathbf{L} \mathbf{q}_z), \quad (10)$$

where $\mathbf{q}^* = [(\mathbf{q}_x^*)^\top (\mathbf{q}_y^*)^\top (\mathbf{q}_z^*)^\top]^\top$, $\mathbf{q} = [\mathbf{q}_x^\top \mathbf{q}_y^\top \mathbf{q}_z^\top]^\top$, $\mathbf{p} = [\mathbf{p}_x^\top \mathbf{p}_y^\top \mathbf{p}_z^\top]^\top$, and $\gamma > 0$ is a regularization parameter. Since (10) is a quadratic programming (QP) problem, its solution can be obtained by solving the following system of linear equations:

$$(\mathbf{I} + \gamma \bar{\mathbf{L}}) \mathbf{q}^* = \mathbf{p}, \quad (11)$$

where $\bar{\mathbf{L}} = \text{diag}\{\mathbf{L}, \mathbf{L}, \mathbf{L}\}$. Since \mathbf{L} is a positive semi-definite (PSD) matrix by definition [38], one can easily see that $\bar{\mathbf{L}}$ is

Table I: Fourteen features created for the i -th point in a given point cloud.

Feature symbol	Explanation
f_1^i	v_i . See (7) and Section III-B2.
f_2^i	x coordinate of $\tilde{\mathbf{p}}_i$. See (5) and Section III-B1.
f_3^i	y coordinate of $\tilde{\mathbf{p}}_i$. See (5) and Section III-B1.
f_4^i	z coordinate of $\tilde{\mathbf{p}}_i$. See (5) and Section III-B1.
f_5^i	x coordinate of $\tilde{\mathbf{p}}_i$. See (6) and Section III-B1.
f_6^i	y coordinate of $\tilde{\mathbf{p}}_i$. See (6) and Section III-B1.
f_7^i	z coordinate of $\tilde{\mathbf{p}}_i$. See (6) and Section III-B1.
f_8^i	\bar{v}_i . See (8) and Section III-B2.
f_9^i	\bar{v}_i . See (9) and Section III-B2.
f_{10}^i	Euclidean distance between point i and the centroid of the point cloud.
f_{11}^i	The number of points inside a ball of radius r and center \mathbf{p}_i .
f_{12}^i	h_i . See Section III-B3.
f_{13}^i	\bar{h}_i . See Section III-B3.
f_{14}^i	\tilde{h}_i . See Section III-B3.

also a PSD matrix. Hence $(\mathbf{I} + \gamma \bar{\mathbf{L}})$ is a *positive definite* (PD) matrix for $\gamma > 0$ and thus invertible.

Moreover, we define another graph signal $\mathbf{h} = [h_1 \dots h_n]$, where $h_i = \|\mathbf{p}_i - \mathbf{q}_i^*\|_2$. Here, $\mathbf{q}_i^* \in \mathbb{R}^3$ is x, y, z coordinates of the LPF coordinates at point i obtained from (11). Further, similar to (8) and (9), we can compute the weighted average signal value at node i and the second difference of \mathbf{h} at node i (denoted as \bar{h}_i and \tilde{h}_i , respectively.) Then, we consider h_i , \bar{h}_i and \tilde{h}_i are the third set of graph-based features at point i .

In addition to the aforementioned graph-based features, we compute following two features for each point i :

- 1) Euclidean distance between point i and the centroid of the corresponding point cloud.
- 2) The number of points inside a ball of radius r and center \mathbf{p}_i . In this paper, we manually choose $r = 0.1$.

Altogether, we have created fourteen features (denoted as $\{f_j^i | j = 1, \dots, 14\}$) for any given point i , as summarized in Table I. These are: the edge intensity value (f_1^i), weighted average of 3D coordinates around neighboring points (f_2^i, f_3^i, f_4^i), second difference of 3D coordinates (f_5^i, f_6^i, f_7^i), the weighted average of edge intensity values around neighboring points (f_8^i), the second difference of edge intensity values (f_9^i), the distance from the centroid (f_{10}^i), the number of points inside a ball of radius $r = 0.1$ (f_{11}^i), the distance between actual 3D points and the low-pass-filtered (LPF) 3D points (f_{12}^i), the weighted average of LPF distance around neighbors (f_{13}^i) and the second difference of LPF distance (f_{14}^i).

IV. FEATURE ANALYSIS

In this section, we present a methodology to examine how well the features introduced in Section III are able to predict adversarial drop points. First, each point is assigned an *adversarial score* that reflects how much it contributes to the corresponding model's prediction. Then, multiple linear regression is used to examine how predictive are various features of the adversarial score.

A. Adversarial score

A point cloud $\mathbf{P} \in \mathbb{R}^{n \times 3}$ is a set of n points in a 3D space, defined as $\mathbf{P} = \{\mathbf{p}_i | i = 1, 2, \dots, n\}$, where each point, \mathbf{p}_i , is represented by its x-y-z coordinates. Let $F : \mathbb{R}^{n \times 3} \rightarrow \{1, 2, \dots, C\}$ be a trained C -class classifier, which maps an input point cloud \mathbf{P} to a class $c_t \in \{1, 2, \dots, C\}$, such that $F(\mathbf{P}) = c_t$. An adversarial attack aims to deceive the classifier by changing the point cloud \mathbf{P} to \mathbf{P}^{adv} so that $F(\mathbf{P}^{adv}) \neq c_t$, while usually also requiring $\mathbf{P}^{adv} \approx \mathbf{P}$.

Saliency score (1) is an indicator of the sensitivity of the classifier to a perturbation of an input point. It has been shown [7] to be effective in determining adversarial points, in the sense that perturbing or removing points with high saliency score can create adversarial examples. One issue with the saliency score is that its dynamic range can be variable. Hence, we define our adversarial score by normalizing the saliency score to the range $[0, 1]$. Specifically, for the i -th point \mathbf{p}_i , we define the adversarial score as

$$z(\mathbf{p}_i) = \frac{s_i - \min\{s_1, \dots, s_n\}}{\max\{s_1, \dots, s_n\} - \min\{s_1, \dots, s_n\}}, \quad (12)$$

where s_i is given in (1). In the next section, we examine how well our fourteen features are able to predict $z(\mathbf{p}_i)$.

B. Multiple linear regression

We employ multiple linear regression analysis [39], [40] to examine how predictive are the features defined in Section III of the adversarial score $z(\mathbf{p}_i)$ in (12). Note that this idea may seem strange to start with: $z(\mathbf{p}_i)$ depends on the classifier model, via the loss \mathcal{L} in the saliency score s_i in (1), while the features in Section III do not! Yet, as the results will show, our features are fairly predictive of $z(\mathbf{p}_i)$.

For a given point \mathbf{p}_i , its adversarial score $z(\mathbf{p}_i)$ and its features $\{f_j^i | j = 1, \dots, 14\}$, we set up the following multiple linear regression model:

$$z(\mathbf{p}_i) \approx \sum_{j=1}^{14} c_j \cdot f_j^i, \quad (13)$$

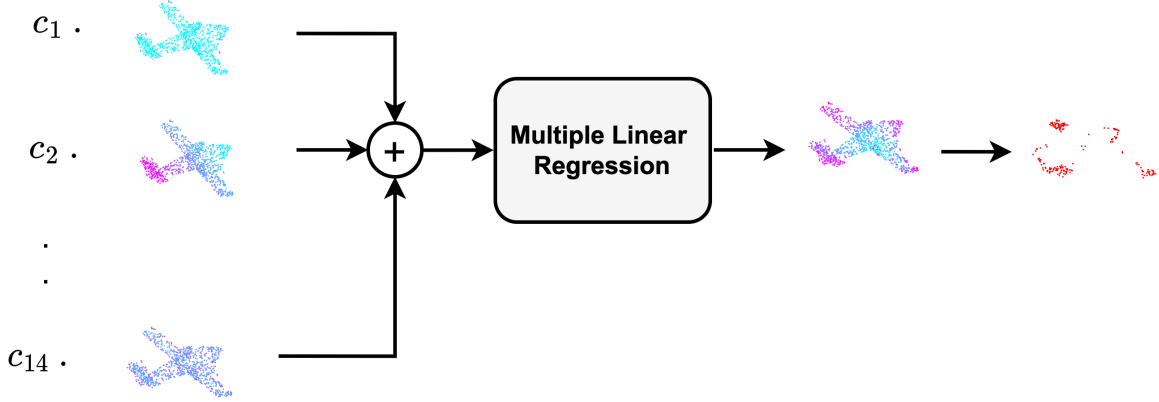


Figure 1: An overview of multiple linear regression analysis. Fourteen features are computed for each point in the point cloud. In the figure, feature values are represented with different colors, with purple corresponding to high values and light blue corresponding to low values. At each point, features are linearly combined using the coefficients estimated on the training data, whose significance is determined using statistical testing. In the final experiment, the N points with the highest predicted score are compared against the N points with the highest true adversarial score.

where c_j are the regression coefficients. An illustration is shown in Fig. 1. The coefficients will be fitted on a set of points from a dataset of point clouds. Naturally, there is a variation in the coefficient values across different point clouds. To determine whether a particular feature is predictive of $z(\mathbf{p}_i)$, we run the following hypothesis test for each coefficient c_j as a t-test [39]:

$$\begin{aligned} H_0 : c_j &= 0, \\ H_1 : c_j &\neq 0. \end{aligned} \quad (14)$$

Here, the null hypothesis H_0 is $c_j = 0$. If the null hypothesis cannot be rejected for a particular coefficient c_j , it means that, given the variation, the coefficient is not significantly different from zero. The interpretation would be that the corresponding feature f_j^i does not contribute to predicting the adversarial score $z(\mathbf{p}_i)$. On the other hand, for coefficients c_j where the null hypothesis can be rejected, we can conclude that the corresponding feature f_j^i is predictive of $z(\mathbf{p}_i)$. As will be seen in the results in the next section, some features are predictive of $z(\mathbf{p}_i)$, others are not.

V. EXPERIMENTS

A. Experimental setting

We used the aligned benchmark ModelNet40¹ dataset, which contains 40 object classes. The dataset was split into 1974 point clouds (objects) for training, and 494 3D objects for testing. Each object contains 1000 points. Three models – PointNet, PointNet++, and DGCNN, with implementation from [11] – were used as deep classifiers on the ModelNet40 dataset. The approach from [7] was used to compute saliency scores (1) iteratively. Specifically, [7] was used to compute the saliency scores for the initial point cloud, then 10 points with the highest score were removed, then this was repeated for the

remaining points until a total of N points were identified. Once the N points with the highest saliency score were identified, their adversarial score $z(\mathbf{p}_i)$ was computed as in (12). All experiments were conducted using PyTorch on a machine with a NVIDIA Tesla P100-PCie card with 16 GB of memory.

B. Multiple linear regression analysis

Fig. 2 shows a visualization of the fourteen features defined in Section III on the airplane object. Each point’s color reflects the value of the corresponding feature at that point, with purple indicating high values and light blue indicating low values.

Saliency scores s_i in (1), and therefore also the adversarial scores $z(\mathbf{p}_i)$ in (12), tend to be most reliable when s_i is high. Therefore, we applied multiple linear regression analysis only to the N points with the highest scores, where $N \in \{50, 100, 150, 200\}$. Fig. 3 shows a visualization of the 100 points with the highest adversarial score, computed from saliency scores of three models: PointNet, PointNet++ and DGCNN. An interesting observation is that, while each network is different, the adversarial points tend to cluster in specific regions like the tail, wings, and tips. Comparing Figs. 2 and 3, we can also see that some features might be indicative of the adversarial points.

To formally test this idea, we use multiple linear regression analysis, specifically the `scikit-learn`² implementation. For each object in the training set, we select N points with the highest adversarial score $z(\mathbf{p}_i)$, then fit the regression model (13). Hypothesis test (14) is run for each coefficient c_j to see whether the null hypothesis can be rejected at the significance level of $\alpha = 0.05$ [39]. Those coefficients for which the null hypothesis can be rejected are deemed significantly different from zero, and the corresponding feature is regarded as sufficiently explanatory for $z(\mathbf{p}_i)$. Other coefficients, for

¹<https://modelnet.cs.princeton.edu/download.html>

²<https://scikit-learn.org/stable/>

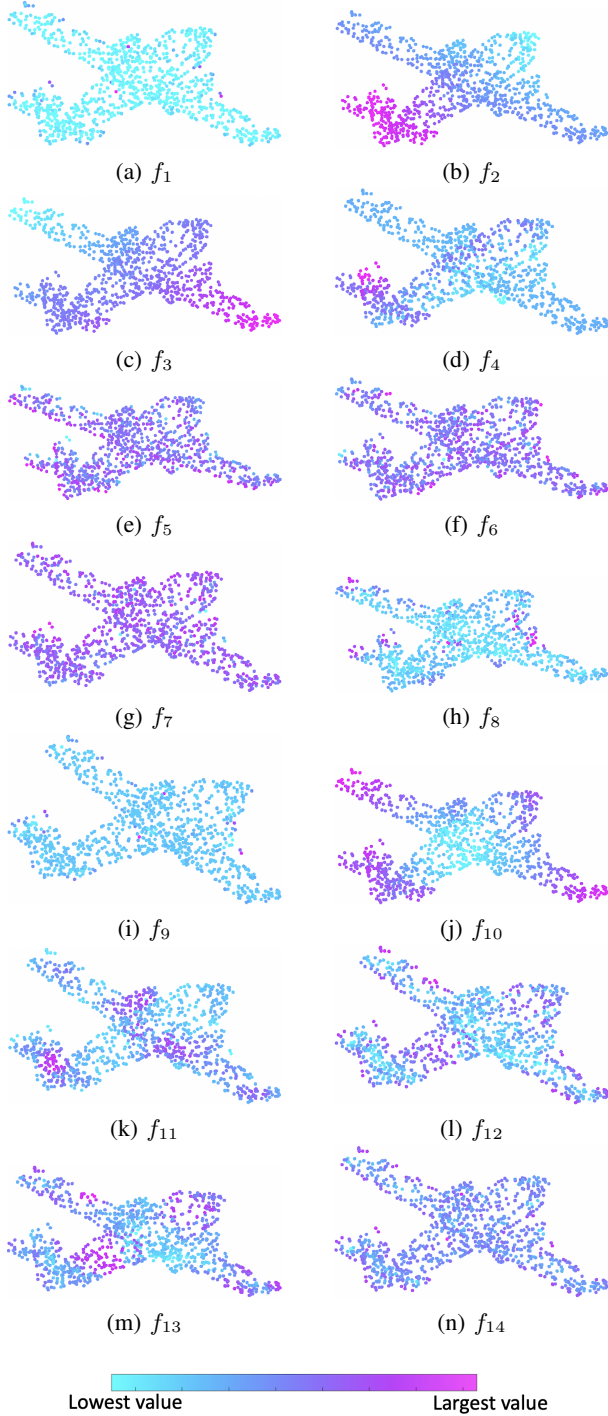


Figure 2: Visualization of 14 features. Points are colorized by the feature value at each point, according to the shown color map.

which the null hypothesis cannot be rejected at the significance level of $\alpha = 0.05$ are deemed insignificant, and the corresponding features regarded as not sufficiently explanatory for $z(\mathbf{p}_i)$. This procedure is repeated for $N \in \{50, 100, 150, 200\}$. The results are shown in Tables II, III, and IV for PointNet, PointNet++, and DGCNN, respectively.

Consider Table II first. For $N \in \{50, 100\}$, four coefficients are insignificant: c_3 , c_5 , c_6 , and c_7 , while the others are

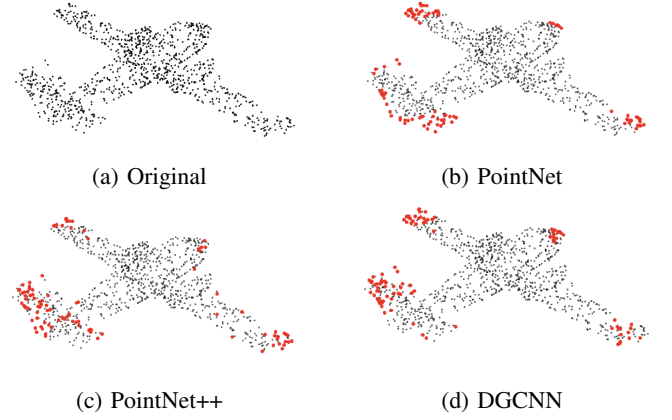


Figure 3: Illustration of adversarial points on the airplane object; (b), (c), and (d) show the 100 points with the highest adversarial score obtained using the corresponding network.

significant at $\alpha = 0.05$. The last column contains the R^2 coefficient of determination [39], shown as a percentage. We can see that R^2 is close to 94%, which is fairly high and indicates good agreement between the data and the model. When the number of points is increased to $N \in \{150, 200\}$, coefficient c_3 becomes significant, and R^2 drops slightly. With the larger number of points, it becomes harder for the model to fit the data (hence the drop in R^2) and an additional feature becomes necessary (hence c_3 becomes significant). Similar behavior can be seen in Tables III and IV as well, although in these cases, c_3 is significant even with $N = 50$ points.

All in all, the results in Tables II, III, and IV show that 10-11 features (f_1 , f_2 , f_4 , f_8 to f_{14} , and sometimes f_3) are indicative of the adversarial score $z(\mathbf{p}_i)$. For example, if we were to predict the adversarial score derived from PointNet for the top $N = 150$ points, then based on the corresponding row in Table II, we could use the following linear model:

$$\begin{aligned} z(\mathbf{p}_i) \approx & -48.596 \cdot f_1^i + 0.006 \cdot f_2^i - 0.002 \cdot f_3^i \\ & - 0.012 \cdot f_4^i - 1.600 \cdot f_8^i + 5.359 \cdot f_9^i \\ & + 0.645 \cdot f_{10}^i + 0.008 \cdot f_{11}^i - 1.954 \cdot f_{12}^i \\ & + 10.266 \cdot f_{13}^i + 0.061 \cdot f_{14}^i. \end{aligned} \quad (15)$$

Although the best coefficients are different for different cases (i.e., different N 's and tables), it is noticeable that the coefficient values do not change too much - they are the same order of magnitude across all cases.

To examine how accurately the regression model predicts the true adversarial scores, we show four graphs in Fig. 4. These graphs correspond to four point clouds whose adversarial scores were computed based on PointNet. The blue scatter plots show $N = 100$ points as pairs of values (Predicted, True), where Predicted is the adversarial score predicted by the linear model (13), while True is the true adversarial score (12). Ideally, if predictions were perfect, the blue points would all fall on the straight red line. While this is not the case in practice, we see that they are close and, more importantly, that the rank order is mostly preserved. This means that if we were looking for the N points with the highest true adversarial

Table II: Multiple linear regression analyses for $N \in \{50, 100, 150, 200\}$ points with the highest adversarial score derived from PointNet. Significant coefficients (at $\alpha = 0.05$) are shown with 3 decimal points precision, while insignificant coefficients are shown as 0.

N	c_1	c_2	c_3	c_4	c_5	c_6	c_7	c_8	c_9	c_{10}	c_{11}	c_{12}	c_{13}	c_{14}	R^2 (%)
50	-47.514	0.008	0	-0.014	0	0	0	-3.462	5.288	0.671	0.009	-2.364	11.182	0.091	94.1%
100	-43.394	0.007	0	-0.012	0	0	0	-9.198	4.895	0.662	0.009	-2.217	10.776	0.081	94.0%
150	-48.596	0.006	-0.002	-0.012	0	0	0	-1.600	5.359	0.645	0.008	-1.954	10.266	0.061	93.9%
200	-48.021	0.006	-0.002	-0.010	0	0	0	-0.764	5.333	0.628	0.008	-1.852	9.932	0.052	93.7%

Table III: Multiple linear regression analyses for $N \in \{50, 100, 150, 200\}$ points with the highest adversarial score derived from PointNet++. Significant coefficients (at $\alpha = 0.05$) are shown with 3 decimal points precision, while insignificant coefficients are shown as 0.

N	c_1	c_2	c_3	c_4	c_5	c_6	c_7	c_8	c_9	c_{10}	c_{11}	c_{12}	c_{13}	c_{14}	R^2 (%)
50	-42.856	0.008	-0.004	-0.011	0	0	0	-9.070	5.008	0.681	0.009	-2.384	11.087	0.086	94.1%
100	-36.936	0.006	-0.003	-0.011	0	0	0	-12.609	4.323	0.663	0.009	-2.455	10.919	0.102	94.0%
150	-42.281	0.006	-0.004	-0.012	0	0	0	-5.667	4.770	0.645	0.008	-2.154	10.413	0.080	93.9%
200	-45.904	0.006	-0.004	-0.011	0	0	0	-0.386	5.041	0.627	0.008	-1.916	9.948	0.063	93.7%

Table IV: Multiple linear regression analyses for $N \in \{50, 100, 150, 200\}$ points with the highest adversarial score derived from DGCNN. Significant coefficients (at $\alpha = 0.05$) are shown with 3 decimal points precision, while insignificant coefficients are shown as 0.

N	c_1	c_2	c_3	c_4	c_5	c_6	c_7	c_8	c_9	c_{10}	c_{11}	c_{12}	c_{13}	c_{14}	R^2 (%)
50	-35.907	0.004	-0.005	-0.010	0	0	0	-14.777	4.201	0.676	0.009	-2.272	10.970	0.088	94.1%
100	-34.385	0.004	-0.003	-0.011	0	0	0	-15.941	4.151	0.662	0.009	-2.667	11.153	0.116	94.0%
150	-41.430	0.003	-0.004	-0.011	0	0	0	-7.817	4.746	0.646	0.008	-2.118	10.390	0.074	93.9%
200	-43.644	0.004	-0.003	-0.010	0	0	0	-4.659	4.932	0.630	0.008	-1.992	10.048	0.065	93.7%

score, we could find many of them by computing the predicted score from the features, and taking N points with the highest predicted score.

To test this idea further, we compute the overlap between the set of top- N points according to the true adversarial score (12) and the set of top- N points according to the predicted adversarial score (13). The results are shown in Fig. 5. The three graphs correspond to the three networks (PointNet, PointNet++, and DGCNN) based on which the true adversarial scores are computed. Each graph shows the percentage overlap for $N \in \{50, 100, 150, 200\}$, for the prediction based on proposed features, as well as a random selection of points. The gap between the two lines indicate how much better is the prediction based on the proposed features compared to a random guess. As seen in the graphs, the prediction based on the proposed features is about 25-30% better than a random guess, and achieves over 50% overlap with the true adversarial drop points for $N = 200$.

C. Visualizations

Finally, we show several visualizations of true and predicted adversarial drop points in Fig. 6. The 100 points with the highest adversarial score computed based on PointNet are shown as red in the three point clouds on the left, while other points are shown as gray. The middle column shows the 100 points with the highest predicted adversarial score based on the proposed features, using the linear model (13) with the coefficients from Table II for $N = 100$. Comparing with the red points in three clouds on the left, we see very good agreement. For example, true and predicted adversarial points tend to concentrate near the chair legs and edges of the seat (top cloud), tip and sides of the cone (middle cloud),

legs and corners (bottom cloud). The last column highlights 100 randomly selected points, which are spread all over the corresponding clouds. Clearly, our feature-based prediction is much closer to the ground-truth adversarial points than a random guess.

VI. CONCLUSION

In point clouds, adversarial drop points whose removal is supposed to fool a given DNN are normally determined using that DNN. In this paper, we presented a novel viewpoint on the problem, and showed that such points can be predicted even without the target DNN model, which we termed a *model-free* approach. To this end, we defined a set of fourteen point cloud features, and examined their ability to predict an adversarial point score using multiple regression analysis. Eleven of the fourteen features were found to be sufficiently predictive of the adversarial score; among them are features that characterize point density, edges, and geometric high-frequency components. These identified features highlight the important characteristics of point clouds that are crucial for their analysis, regardless of the DNN model that analyzes them. This was demonstrated by testing how well the feature-based approach is able to identify adversarial drop points of three well-known DNNs: PointNet, PointNet++, and DGCNN. In all cases, the feature-based approach performed much better than a random guess. One implication of this work is that the geometry of data instances, and not just data distribution, is important for adversarial attacks, and this insight could help devise better defenses.

ACKNOWLEDGEMENTS

This work was partly supported by a grant from Iran National Science Foundation (INSF) and the Natural Sciences

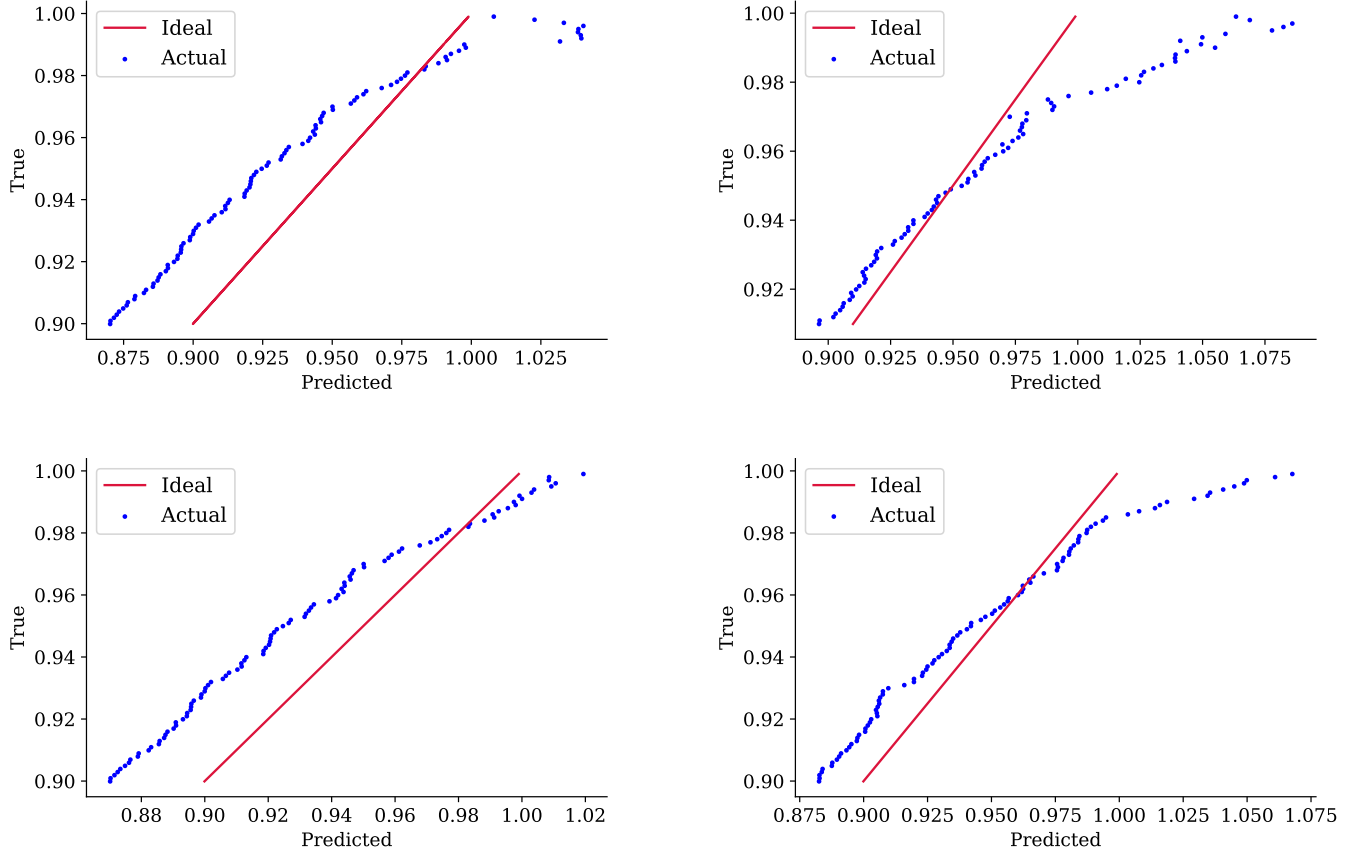


Figure 4: Predicted vs. true adversarial scores for four point clouds. Perfect prediction would correspond to the straight red line, actual predictions give blue scatter plots.

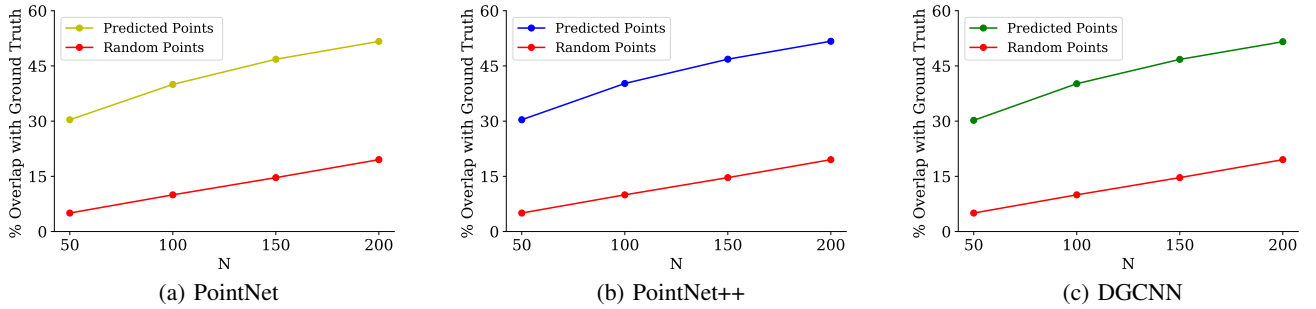


Figure 5: A comparison of ground truth adversarial points generated by (a) PointNet, (b) PointNet++, and (c) DGCNN with feature-based predicted points and random points.

and Engineering Research Council (NSERC) of Canada.

REFERENCES

- [1] I. J. Goodfellow, J. Shlens, and C. Szegedy, “Explaining and harnessing adversarial examples,” *arXiv preprint arXiv:1412.6572*, 2014.
- [2] C. Szegedy, W. Zaremba, I. Sutskever, J. Bruna, D. Erhan, I. J. Goodfellow, and R. Fergus, “Intriguing properties of neural networks,” *arXiv preprint arXiv:1312.6199*, 2013.
- [3] S.-M. Moosavi-Dezfooli, A. Fawzi, O. Fawzi, and P. Frossard, “Universal adversarial perturbations,” in *Proc. IEEE/CVF CVPR*, 2017, pp. 1765–1773.
- [4] N. Carlini and D. Wagner, “Towards evaluating the robustness of neural networks,” in *Proc. IEEE Symp. Security and Privacy*, 2017, pp. 39–57.
- [5] D. Liu, R. Yu, and H. Su, “Extending adversarial attacks and defenses to deep 3d point cloud classifiers,” in *Proc. IEEE ICIP*, 2019, pp. 2279–2283.
- [6] C. Xiang, C. R. Qi, and B. Li, “Generating 3D adversarial point clouds,” in *Proc. IEEE/CVF CVPR*, 2019, pp. 9136–9144.
- [7] T. Zheng, C. Chen, J. Yuan, B. Li, and K. Ren, “Pointcloud saliency maps,” in *Proc. IEEE/CVF ICCV*, 2019, pp. 1598–1606.
- [8] B. Zhang, S. Huang, W. Shen, and Z. Wei, “Explaining the PointNet: what has been learned inside the PointNet?,” in *Proc. IEEE/CVF CVPR Workshops*, 2019, pp. 71–74.
- [9] S. Fan, W. Gao, and G. Li, “Salient object detection for point clouds,” *arXiv preprint arXiv:2207.11889*, 2022.
- [10] J. Yang, Q. Zhang, R. Fang, B. Ni, J. Liu, and Q. Tian, “Adversarial attack and defense on point sets,” *arXiv preprint arXiv:1902.10899*,

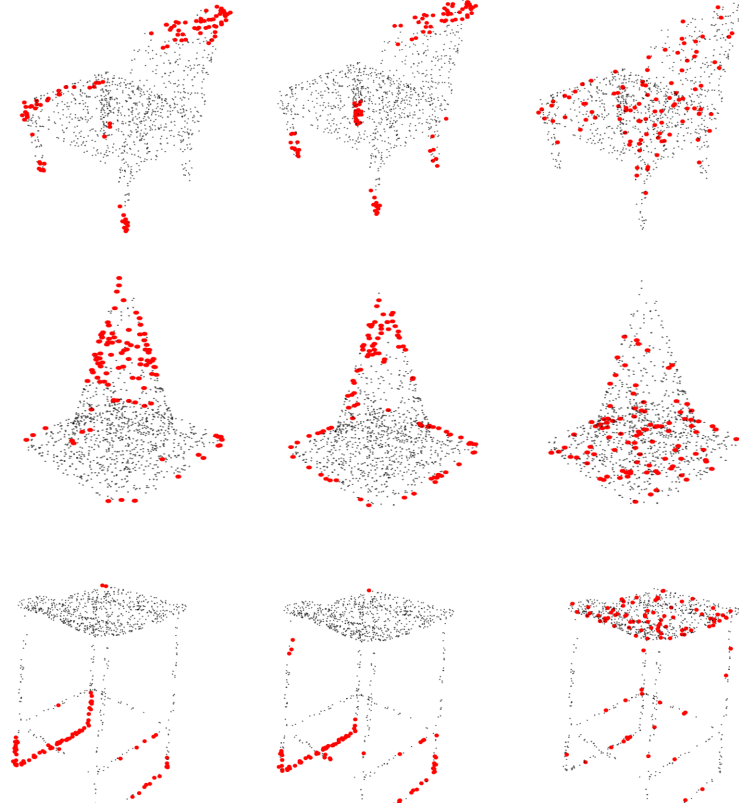


Figure 6: Visualisation of adversarial point prediction, where (predicted) adversarial points are shown in red, and the other points in the cloud as gray. (Left) 100 points with the highest true adversarial score computed based on PointNet. (Middle) 100 points with the highest predicted adversarial score computed using the proposed features. (Right) 100 randomly selected points.

- 2021.
- [11] Z. Wu, Y. Duan, H. Wang, Q. Fan, and L. J. Guibas, “If-defense: 3D adversarial point cloud defense via implicit function based restoration,” *arXiv preprint arXiv:2010.05272*, 2020.
- [12] H. Naderi, A. Etemadi, K. Noorbakhsh, and S. Kasaei, “LPF-defense: 3D adversarial defense based on frequency analysis,” *arXiv preprint arXiv:2202.11287*, 2022.
- [13] H. Zhou, K. Chen, W. Zhang, H. Fang, W. Zhou, and N. Yu, “DUP-Net: denoiser and upsampler network for 3D adversarial point clouds defense,” in *Proc. IEEE/CVF ICCV*, 2019, pp. 1961–1970.
- [14] A. Ilyas, S. Santurkar, D. Tsipras, L. Engstrom, B. Tran, and A. Madry, “Adversarial examples are not bugs, they are features,” in *Advances in Neural Information Processing Systems*, 2019, pp. 125–136.
- [15] C. R. Qi, H. Su, K. Mo, and L. J. Guibas, “PointNet: Deep learning on point sets for 3D classification and segmentation,” in *Proc. IEEE/CVF CVPR*, 2017, pp. 652–660.
- [16] C. R. Qi, L. Yi, H. Su, and L. J. Guibas, “PointNet++: Deep hierarchical feature learning on point sets in a metric space,” *arXiv preprint arXiv:1706.02413*, 2017.
- [17] Y. Wang, Y. Sun, Z. Liu, S. E. Sarma, M. M. Bronstein, and J. M. Solomon, “Dynamic graph CNN for learning on point clouds,” *ACM Trans. Graphics*, vol. 38, no. 5, pp. 1–12, 2019.
- [18] A. Madry, A. Makelov, L. Schmidt, D. Tsipras, and A. Vladu, “Towards deep learning models resistant to adversarial attacks,” *arXiv preprint arXiv:1706.06083*, 2017.
- [19] Tzungyu Tsai, Kaichen Yang, Tsung-Yi Ho, and Yier Jin, “Robust adversarial objects against deep learning models,” in *Proceedings of the AAAI Conference on Artificial Intelligence*, 2020, vol. 34, pp. 954–962.
- [20] J. Kim, B.-S. Hua, T. Nguyen, and S.-K. Yeung, “Minimal adversarial examples for deep learning on 3D point clouds,” in *Proc. IEEE/CVF ICCV*, 2021, pp. 7797–7806.
- [21] M. Wicker and M. Kwiatkowska, “Robustness of 3D deep learning in an adversarial setting,” in *Proc. IEEE/CVF CVPR*, 2019, pp. 11767–11775.
- [22] A. Arya, H. Naderi, and S. Kasaei, “Adversarial attack by limited point cloud surface modifications,” *arXiv preprint arXiv:2110.03745*, 2021.
- [23] D. Liu, R. Yu, and H. Su, “Adversarial point perturbations on 3D objects,” *arXiv preprint arXiv:1908.06062*, 2019.
- [24] A. V. Phan, M. Le Nguyen, Y. L. H. Nguyen, and L. T. Bui, “DGCNN: A convolutional neural network over large-scale labeled graphs,” *Neural Networks*, vol. 108, pp. 533–543, 2018.
- [25] D. I. Shuman, S. K. Narang, P. Frossard, Antonio A. Ortega, and P. Vandergheynst, “The emerging field of signal processing on graphs: Extending high-dimensional data analysis to networks and other irregular domains,” *IEEE Signal Process. Mag.*, vol. 30, no. 3, pp. 83–98, 2013.
- [26] X. Liu, G. Cheung, X. Wu, and D. Zhao, “Random walk graph laplacian-based smoothness prior for soft decoding of jpeg images,” *IEEE Trans. Image Process.*, vol. 26, no. 2, pp. 509–524, Feb 2017.
- [27] A. Ortega, P. Frossard, J. Kovacevic, J. M. F. Moura, and P. Vandergheynst, “Graph signal processing: Overview, challenges, and applications,” *Proc. IEEE*, vol. 106, no. 5, pp. 808–828, May 2018.
- [28] S. Chen, D. Tian, C. Feng, A. Vetro, and J. Kovacevic, “Fast resampling of three-dimensional point clouds via graphs,” *IEEE Trans. Signal Process.*, vol. 66, no. 3, pp. 666–681, Feb 2018.
- [29] G. Cheung, E. Magli, Y. Tanaka, and M. K. Ng, “Graph spectral image processing,” *Proc. IEEE*, vol. 106, no. 5, pp. 907–930, May 2018.
- [30] C. Dinesh, G. Cheung, and I. V. Bajić, “Super-resolution of 3D color point clouds via fast graph total variation,” in *Proc. IEEE ICASSP*, 2020, pp. 1983–1987.
- [31] C. Dinesh, G. Cheung, and I. V. Bajić, “3D point cloud color denoising using convex graph-signal smoothness priors,” in *Proc. IEEE MMSP*, Sep. 2019, pp. 1–6.
- [32] C. Dinesh, G. Cheung, F. Wang, and I. V. Bajić, “Sampling of 3D point

- cloud via Gershgorin disc alignment,” in *Proc. IEEE ICIP*, 2020, pp. 2736–2740.
- [33] W. Hu, X. Gao, G. Cheung, and Z. Guo, “Feature graph learning for 3D point cloud denoising,” *IEEE Trans. Signal Process.*, vol. 68, pp. 2841–2856, 2020.
 - [34] Z. Fu, W. Hu, and Z. Guo, “3D dynamic point cloud inpainting via temporal consistency on graphs,” in *Proc. IEEE ICME*, 2020, pp. 1–6.
 - [35] J. Qi, W. Hu, and Z. Guo, “Feature preserving and uniformity-controllable point cloud simplification on graph,” in *Proc. IEEE ICME*, 2019, pp. 284–289.
 - [36] J. Zeng, G. Cheung, M. Ng, J. Pang, and C. Yang, “3D point cloud denoising using graph laplacian regularization of a low dimensional manifold model,” *IEEE Trans. Image Process.*, vol. 29, pp. 3474–3489, 2020.
 - [37] Y. Schoenenberger, J. Paratte, and P. Vanderghelynst, “Graph-based denoising for time-varying point clouds,” in *IEEE 3DTV-Conference*, 2015, pp. 1–4.
 - [38] F. R. Chung and F. C. Graham, *Spectral graph theory*, American Mathematical Soc., 1997.
 - [39] M. H. Kutner, C. J. Nachtsheim, J. Neter, and W. Li, *Applied Linear Statistical Models*, McGraw-Hill/Irwin, 5th edition, 2005.
 - [40] L. E. Eberly, “Multiple linear regression,” *Topics in Biostatistics*, pp. 165–187, 2007.